Slobodan Stupar
Jovan Isaković
Dragan Komarov
Aleksandar Simonović
Dijana Damljanović

ISSN 1333-1124

COMPUTATIONAL AND EXPERIMENTAL INVESTIGATION INTO SUBSONIC FLOW AROUND A FINNED OGIVE CYLINDER

UDC 533.6:519.6

Summary

Experimental and numerical investigation into the flow around an ogive cylinder with fins (missile calibration model) was conducted for Mach 0.6 flow. The computational results were compared to the results of pressure-distribution and force/moments measurements conducted in the T-38 trisonic blowdown wind tunnel of the Military Technical Institute of Serbia. In addition to the pressure distribution along the model, the base pressure was computed and compared to experimental data. Standard pre-processing techniques and a realizable k-ε turbulence model with enhanced wall treatment were used in the flow computations. The numerical simulation results achieved with moderate hardware resources were found to be in relatively good agreement with the experiment if high separation in the base region and related issues that CFD analysts are faced with are taken into account.

Key words: *subsonic flow, ogive cylinder, wind tunnel, CFD, pressure distribution, base flow, aerodynamic coefficients*

1. Introduction

A series of wind tunnel calibration tests have been conducted on a missile calibration model in the T-38 trisonic blowdown wind tunnel of the Military Technical Institute of Serbia (VTI). The obtained pressure distributions and aerodynamic coefficients for subsonic flow were compared to the computational fluid dynamics (CFD) results.

The compressible flows around ogive slender bodies were thoroughly investigated in experiments carried out during the second half of the last century. Although considerable effort was expended resulting in considerable achievements, there is still space for further investigation into such flows [1, 2, 3]. Instability of shear layers in the aforementioned flows induces strong unsteadiness in the region behind the base [4] which leads to complex experimental measurements that are difficult to conduct and that are related with uncertainties of the results. CFD simulations ought to be combined with an experimental analysis in order to improve both experimental and numerical means of the analysis of compressible flows.

The region of the base flow is of particular interest for such combined studies due to high unsteadiness and sensitivity of experimental results obtained by different techniques. This kind of investigation requires specific experimental apparatus and methods [5] and/or substantial hardware resources and advanced CFD methods in the case of numerical simulations that are able to resolve the flow in greater detail [4, 6, 7]. However, in this paper the authors have tried to obtain acceptable results combining experimental measurements and CFD simulations that are the current industry standard, using moderate hardware resources in terms of widely accessible scientific computing technologies.

Besides wind tunnel tests that play an important role in aeronautical industry, as well as in research sector, CFD has been increasingly used at both levels in the last decades. With advances made in CFD simulations and accompanying hardware development, it is possible to obtain reasonably good results compared to the wind tunnel tests which can be used as an additional source of data used for qualitative and quantitative analyses of flows.

2. Geometry and experiment flow conditions

The missile calibration model configuration consisted of a cylindrical body with a spherically blunted tangent ogive nose, an increase in diameter at the base, and four fins in cruciform configuration. Basic model dimensions, relative to the model base diameter D, are given in Figure 1.

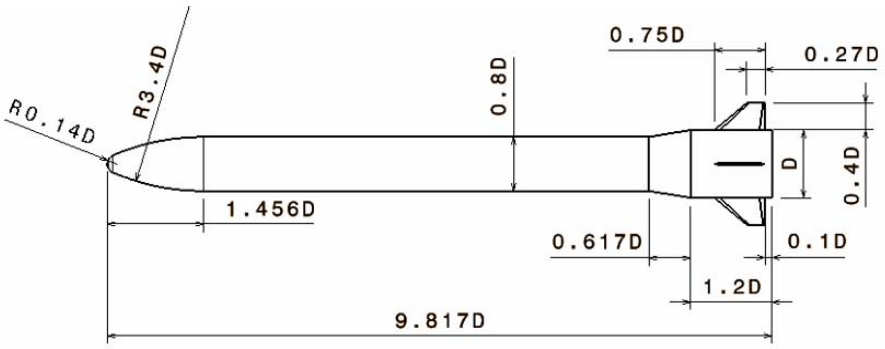

Fig. 1 Geometry of the model configuration

The flow conditions of the wind tunnel tests that were also used in CFD simulations are given in Table 1 (α - angle of attack, Re – Reynolds number reduced to 1m characteristic length, p_{st} – static pressure in the wind tunnel test section, p_o – stagnation pressure in the wind tunnel test section, T_o – stagnation temperature in the wind tunnel test section, p_{dyn} – dynamic pressure in the test section).

Table 1 Flow conditions

Case no.	Ma	α [°]	10^6 Re	p_{st} [bar]	p_o [bar]	T_o [bar]	p_{dyn} [bar]
1	0.601	0	28.75	1.967	2.510	297.2	0.4971
2	0.601	4	28.96	1.963	2.507	294.1	0.4973
3	0.602	8	28.94	1.963	2.508	294.2	0.4990
4	0.602	13	28.94	1.693	2.508	294.2	0.4990
5	0.602	16	28.94	1.963	2.510	294.2	0.4990

3. Test facility

Figure 2 shows the T-38 test facility at the Military Technical Institute. It is a blowdown-type pressurized wind tunnel with a 1.5m x 1.5m square test section. For subsonic and supersonic tests, the test section is with solid walls, while for transonic tests, a section with porous walls is inserted into the wind tunnel configuration.

Mach number in the 0.2 - 4 range can be achieved in the test section, with Reynolds numbers of up to 110 million per meter. Mach number is set and maintained within 0.5% of the nominal value by means of a flexible nozzle or sidewall flaps and/or sidewall blowoff, depending on the test speed range.

Stagnation pressure in the test section can be maintained between 1.1 bar and 15 bar, depending on the Mach number, and regulated to 0.3% of nominal value. Run times are in the range 6s to 60s, depending on the Mach number and stagnation pressure.

The model is supported in the test section by a tail sting mounted on a pitch-and-roll mechanism by which desired aerodynamic angles can be achieved. The facility supports both the step-by-step model movement and the continuous model movement (sweep) during measurements.

Several calibration test programmes are developed in order to verify the quality of the air stream in the test section of the wind tunnel, the condition of instrumentation and the correctness of the data reduction algorithm [8, 9].

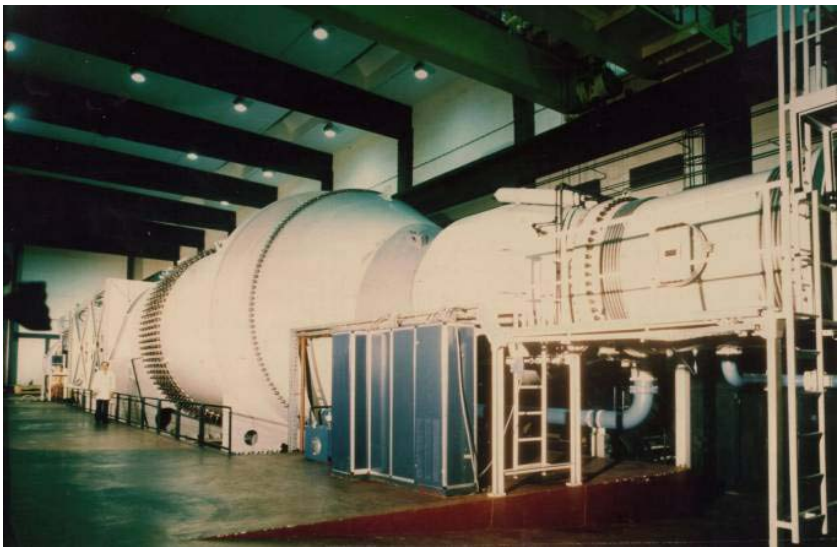

Fig. 2 T-38 test facility at the Military Technical Institute

4. Determination of pressure distribution

Pressure measurement installation was built into the model. It consisted of 40 ports for the measurement of model-surface pressures and steel tubing distributed as follows: 25 ports on 9 sections of model fuselage, 1 port on the model base, 8 ports on a left-fin section, 6 ports on a right-fin section.

Steel tubing from all pressure ports was passed to the front part of the model, then bent and passed through the mode-sting mating adaptor and through the tail sting. An electromechanical scanning device was installed in the model support, behind the tail sting, and connected to the steel tubes coming from the model.

Tubes leading from pressure ports on model sections were connected sequentially to scanning device ports, starting from port 2 and ending at port 41. Ports 1 and 42 were short-

circuited pneumatically to the reference pressure port of the pressure transducer to enable its auto-zeroing in each scan. The wind tunnel test section static pressure was connected to this tubing.

The stagnation pressure in the test section was measured by a Mensor quartz bourdon tube absolute pressure transducer pneumatically connected to a pitot probe in the settling chamber of the wind tunnel. The range of that transducer was 7 bar. The static pressure in the test section was measured by a Mensor quartz bourdon tube differential pressure transducer (with a lower range) pneumatically connected to the stagnation pressure pitot probe and to an orifice on the test section sidewall. The range of that transducer was 1.75 bar. The nonlinearity and hysteresis of the transducers used were typically 0.02% F.S.

The stagnation temperature was measured by a RTD probe in the settling chamber. The accuracy of that transducer was approximately ±0.5K.

The pitching and rolling angles of the model support were measured by resolvers which are a part of the mechanism. The resolution of the pitching angle resolver was 0.05° and of the rolling angle resolver 0.25°.

Pressure distribution was measured using an electromechanical scanning device with a solenoid-driven valve. This type of scanning device features 48 measurement ports with a scanning speed of 10 ports/second. A piezoresistive differential pressure transducer was used to measure local pressures. The nominal range of this transducer was 3.5 bar, but it was calibrated in 1.25 and 2.5 bar ranges (for testing at lower Mach numbers), with 0.05% F.S. nonlinearity and hysteresis.

The data acquisition system consisted of a Teledyne 64 channel "front end" controlled by a computer. The front-end channels for flow parameters transducers were set with 10 Hz, fourth-order low pass Butterworth filters and appropriate amplification. The front-end channel for pressure transducer was set with a 100 Hz low-pass filter of the same type.

The data from all analogue channels were digitized by a 16-bit resolution A/D converter with the overall accuracy of the acquisition system being about 0.05% F.S. of the channel signal range. All channels were sampled with the same 400 samples/s rate.

Digitized data were sent through the network to a data reduction computer and stored on disk for later reduction.

Data reduction was performed after each run, using the T-38 standard software package. The processing was done in several stages, and each stage was performed by a different software module. Stages were as follows: interfacing of data acquisition system and normalization of signals, determination of flow parameters, determination of model position (orientation) and determination of pressure distribution.

The scanning device operates by rotating a valve that connects mode-pressure measuring ports sequentially to a single differential pressure transducer. The main benefit of this concept was that many local pressures could be measured with a single transducer, which greatly simplified the test installation, put less load on the data acquisition system, etc. Main drawbacks were in the fact that the pressures were not measured simultaneously and in the fact that after each port-switching of the rotating valve, some time was required for the pressure to settle in the tubing. The pressure-settling time effectively limited the scanning speed to about 10 ports/second although there was the capability to scan at about 40 ports/second.

In the T-38 wind tunnel test programme, a single scan was performed at each model position (angle of attack, α) in each run. Data reduction was identical for each step.

For each model section, an array of local (differential) pressures was obtained. Once the local differential pressure for each model-section port 'p' had been measured and determined, the absolute local pressure was obtained by adding the reference pressure (test section static pressure). The local pressure coefficient for each port was then calculated by normalizing the difference between the test section static pressure and the dynamic pressure.

5. Determination of aerodynamic coefficients

Aerodynamic coefficients were determined in wind tunnel tests using a force model with the same geometry as that of a model for pressure measurements. Test conditions were the same as those used for pressure-distribution determination. A VTI-produced internal six-component strain gauge balance was used for measurements of forces/moments. Nominal load range of the balance was 3000 N for the normal and side forces, 700 N for the axial force, 200 Nm for the pitching and yawing moments, and 50 Nm for the rolling moment. The nominal accuracy of the balance is 0.2% F.S. for each component. Calibration of the balance showed that it was operational within the nominal design accuracy (actually, an accuracy better than 0.1 % FS was obtained in calibration for all components). In the wind tunnel tests, the balance was mounted on a sting with 40 mm in diameter.

The stagnation pressure in the test section was measured as described in the case of pressure distribution measurement. The stagnation temperature was measured by a RTD probe and the static pressure by a Mensor quartz bourdon tube differential pressure transducer (but lower range) pneumatically connected to the stagnation pressure pitot probe. The base pressure on the model was measured by a Druck PDCR42 piezoresistive differential pressure transducer. The active side of this transducer was connected to an orifice on the sting inside the rear part of the model. The reference side of the transducer was connected to the tubing leading from the static pressure port on the wall of the test section. The range of this transducer was 0.35 bar, with 0.05% F.S. nonlinearity and hysteresis. The pitching and rolling angles of the model support were measured by optical encoders integrated into the model support mechanism. The accuracy of reading was typically 0.02° for both axes.

The previously described data acquisition system was used. The front end channels for flow parameters transducers were set with 10 Hz, fourth-order low pass Butterworth filters and appropriate amplification. The output of a precision digital clock was sampled synchronously with other channels in order to serve as a time base for the segmentation of data.

In order to minimize the differences in time lags on various channels during the model sweep, the channels for six balance components and base pressure were set with 30 Hz low pass filters of the same type. In order to compensate for the poorer filtering on these channels, these signals were additionally filtered during the data reduction by a 3 Hz non-casual low pass digital filter. All channels were sampled with the same 200 samples/s rate.

After having been collected, the data was reduced to the axis system attached to the body – body coordinate system. The origin of this axis system is located at the front of the ogive nose. The X axis was parallel to the longitudinal axis, and positive towards the end of the model, Z axis lay in the plane of symmetry of the model, and the Y axis was directed towards the left side of the model and completed a left-handed axis system.

6. Repeatability and accuracy of measurement

For the type of transducers used in wind tunnel tests, the overall uncertainty of measurement is roughly proportional to a multiple of random error estimated by standard deviation, so the latter was used to express the degree of the measurement accuracy.

Knowing the accuracies of individual sensors it was possible to estimate standard deviations of measurements of various quantities (computed from several independently measured quantities) in the wind tunnel tests (pressure-distribution and measurement of forces/moments).

The standard deviation of pressure-distribution measurement was about 0.0042 for subsonic flows.

Previous pressure distribution measurements in the T-38 wind tunnel have given an insight into the expected repeatability of data. It has been estimated that at subsonic Mach numbers, repeatability of measurements is usually about ±0.005 to 0.01. Repeatability of the main test-section flow parameters (stagnation pressure and Mach numbers) has been estimated to be about 0.5 to 1% of nominal values.

7. Numerical model

The commercial finite-volume solver Fluent v12.1 was used to solve unsteady governing equations for the compressible flow on an unstructured hybrid grid. The solver was density-based [10]. The implicit method for linearization of governing equations was used. The second order upwind discretization was used for pressure, velocity and temperature variables, while the first order discretization was used for turbulent kinetic energy and dissipation rate related to the realizable k-ε turbulence model that was chosen for the closure of Reynolds-averaged Navier-Stokes (RANS) governing equations [11]. The first order implicit temporal discretization was used. Gradients were obtained by the least squares cell-based method, as this method uses less computer resources and its accuracy is comparable to that of the node-based gradient method [12]. The inviscid flux vector was computed by the upwind flux-differencing splitting [13]. The realizable k-ε model was used with enhanced wall treatment in order to resolve the flow in the near wall region.

The computation was initially done on a coarse mesh with a non-dimensional distance from the wall of $y^+ \approx 30$ in order to obtain the flow field that presented a basis for the grid adaptation. Final mesh with the first near-wall node placed at $y^+ \approx 1$ in the whole domain for case no. 1 (angle of attack 0º) had 6.1 million cells. For cases 2 - 5 (angles of attack: 4º, 8º, 13º, and 16º) the first near-wall node was placed at $y^+ \approx 1$ except in the narrow region near trailing edges of the fins where it was $y^+ < 8$, resulting in a grid with 4.9 million cells. The computations for case 1 showed that the results were acceptable for the computation setup with such a grid. The near-wall region was discretized with 23 layers of prismatic cells, while the rest of the flow domain consisted of tetrahedral cells, Figure 3. The mesh growth rate in the near-wall region was 1.15. In the regions where $y^+ \approx 1$, the viscous sub-layer was resolved using a two-layer model for enhanced wall treatment, while the enhanced wall treatment through the blending of linear and logarithmic laws in the near-wall region was used in the regions with a higher y+.

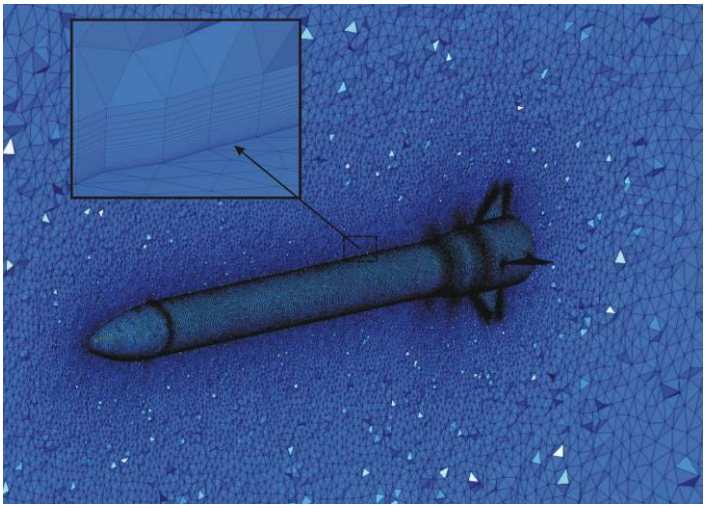

Fig. 3 Computational grid with a detail of the grid in the near-wall region

The cylindrical domain spans 15 model lengths upstream and in the radial direction, while the downstream domain spreads to 20 model lengths. The domain extents have been

halved using the symmetry boundary condition parallel to the symmetry plane of the model. The pressure far-field non-reflecting boundary conditions were implemented upstream, downstream and at the outer cylindrical boundary with flow parameters corresponding to the flow conditions during the wind tunnel tests. The no-slip boundary condition was used at the model walls. The ideal gas hypothesis for air and the Sutherland law for viscosity were used in computations.

The unsteady computations were run until the fluctuations of normal coefficients in two perpendicular directions relative to the longitudinal axis of the model have been stabilized to the level less than 1% of the mean values for the last 100 iterations [14]. The Courant-Fridrichs-Levy (CFL) number in the value of 1 was used at the beginning of the simulation. The value of the CFL number was increased up to 10 during the computations.

8. Results and discussion

The CFD simulations were run for the following angles of attack: 0°, 4°, 8°, 13°, and 16°. In order to compare the wind tunnel test results with CFD computations, computational data was post-processed so that pressure values are obtained in the points corresponding to the location of the pressure ports of the wind tunnel model. The locations of the pressure ports that were used for the comparison are shown in Figure 4 for a cross-section of the model. The same distribution of the pressure ports was used for eight cross-sections located at the nose and the afterbody of the model for the purpose of comparison between the CFD and experimental results. The computed pressure at the tip of the spherically blunted nose was compared to the corresponding pressure obtained at the port on the same location in the experiment, while the experimental value of the base pressure was compared to the computed area weighted base pressure. The base pressure results are shown in Table 2.

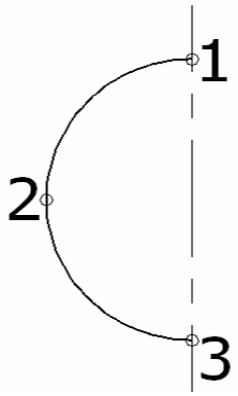

Fig. 4 Location of the points used for the comparison of experimental and numerical results of one of the investigated sections

Certain longitudinal pressure coefficient distributions for CFD simulations shown in Figures 5 – 7 were calculated based on the undisturbed static and dynamic pressures at the far-field boundary that corresponded to the measured values in the wind tunnel test section. The pressure coefficients were calculated as:

$$c_p = \frac{p - p_{st}}{p_{dyn}} \tag{1}$$

where p is the computed pressure corresponding to the location of the pressure port.

The experimental values are denoted with points in the figures. Fairly good agreement has been achieved between the numerical model and the wind tunnel tests for the longitudinal pressure distribution in all cases.

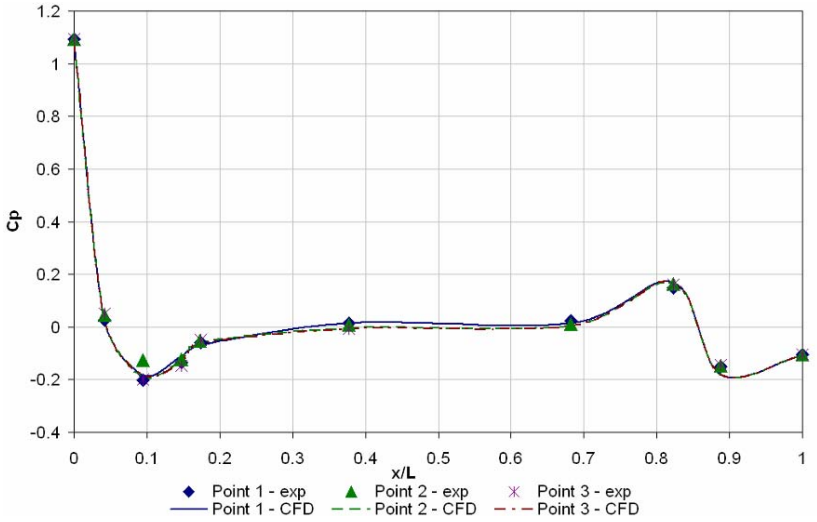

Fig. 5 Pressure coefficients at α = 0°

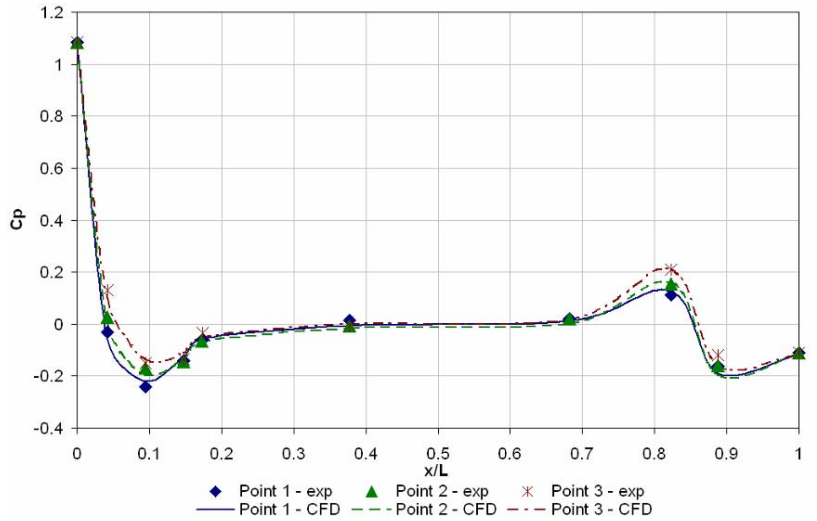

Fig. 6 Pressure coefficients at α = 4°

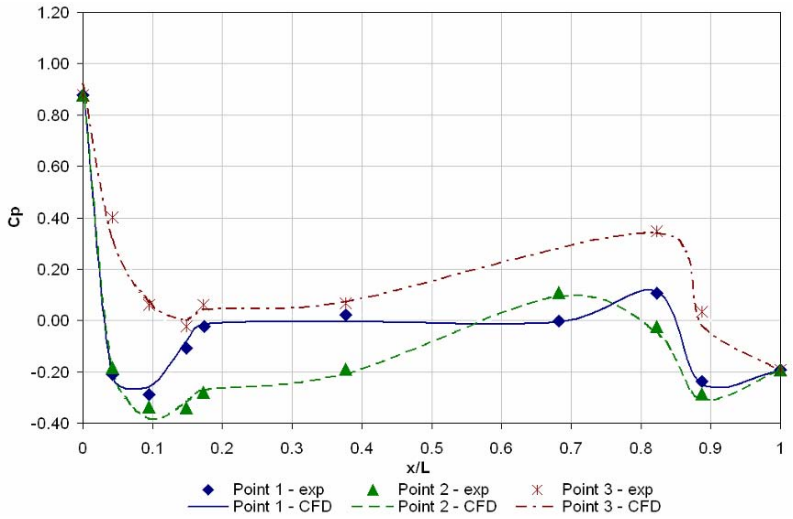

Fig. 7 Pressure coefficients at α = 16°

Table 2 Base pressure coefficients obtained in experiments and in a CFD simulation

α [°]	0	4	8	13	16
$c_{pbase,exp}$	-0.106	-0.111	-0.123	-0.1535	-0.1830
$c_{pbase,CFD}$	-0.111	-0.117	-0.1396	-0.1587	-0.1962

Velocity vectors and pressure fields are shown for the symmetry cross-section of the base region for the three flow cases in Figures 8-10. The recirculation regions with lower pressure are clearly identified, as well as the stagnation points and the regions of higher pressure further downstream. The point of maximum pressure in the recirculation region for the case 1 (angle of attack 0º) is 1.88D behind the base. This pressure is 4.3% higher than the free-stream pressure, which corresponded well to the results obtained by using a more complex CFD method [4]. The maximum Mach number on the centre-line of the wake is 0.23 placed at 0.94D behind the base for the case 1. For the same flow case, the downstream static pressure equal to the free-stream pressure is found at approximately 8.5D behind the base. The points of maximum pressure for the cases of other two angles of attack are displaced with respect to the wake centre-line, as expected.

The shear layers in the base flow can be identified in Figures 8 -10 as well as in Figures 11 - 13. The intense vorticity regions are shown. In spite of the fact that the grid resolution in the shear layer is insufficient for a detailed analysis of the phenomena in the proximity of this region, such as interactions with the recirculation region as well as the outer region of the flow, the results are sufficient for the identification of recirculation and shear layer regions.

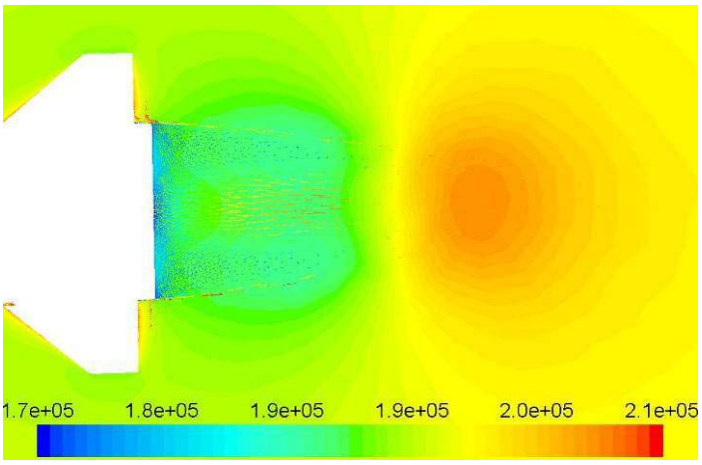

Fig. 8 Pressure field and velocity vectors behind the model base at α = 0º

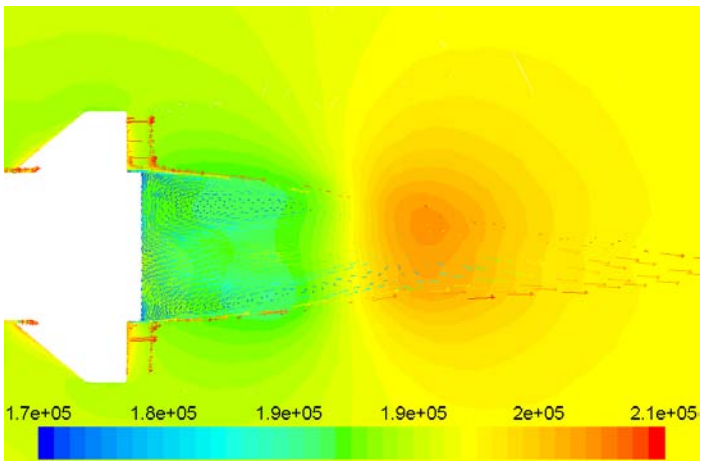

Fig. 9 Pressure field and velocity vectors behind the model base at α = 4º

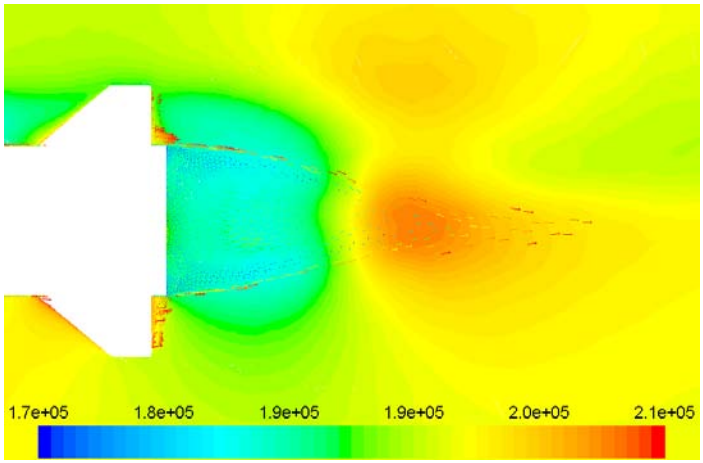

Fig. 10 Pressure field and velocity vectors behind the model base at α = 16º

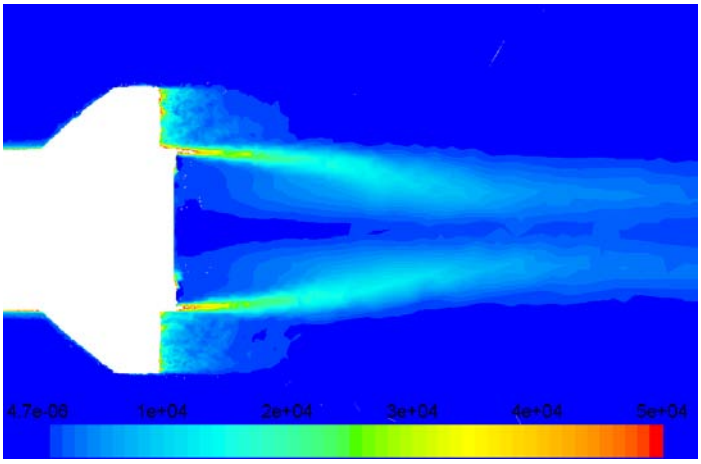

Fig. 11 Vorticity magnitude behind the base at α = 0º with the recirculation region shown

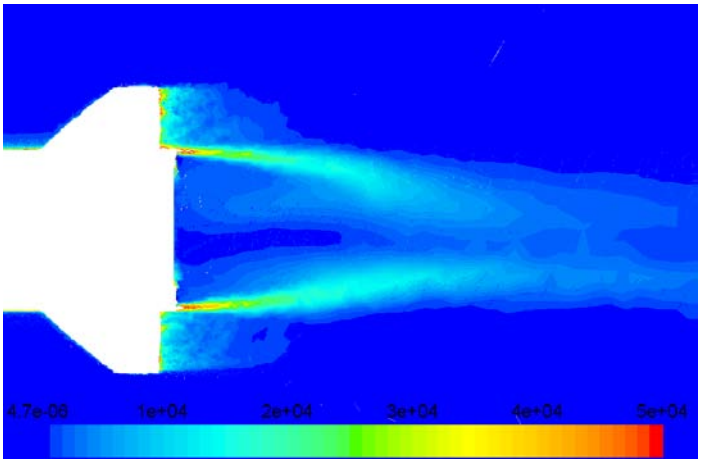

Fig. 12 Vorticity magnitude behind the base at α = 4º with the recirculation region shown

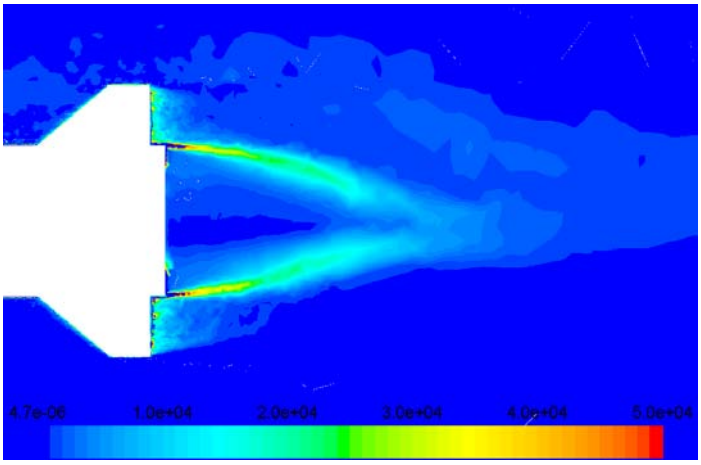

Fig. 13 Vorticity magnitude behind the base at α = 16º with the recirculation region shown

The reference area for the calculation of c_a (axial force coefficient) and c_n (normal force coefficient) is the area of the model base. The aerodynamic coefficients were reduced to the body axis coordinate system. The model reference length is the model base diameter D and the moment reference point is 5.6932D aft of the missile nose.

Table 3 Aerodynamic coefficients obtained in experiments and CFD simulations (in the body axis system)

α [º]	0	4	8	13	16
$c_{a,\,exp}$	0.1747	0.1707	0.1764	0.1826	0.2044
$c_{a,CFD}$	0.1788	0.1775	0.1852	0.1904	0.2191
$c_{n,exp}$	-0.009	0.342	0.746	1.294	1.612
$c_{n,CFD}$	0.0013	0.3503	0.7494	1.1709	1.3301
$c_{m,exp}$	0.009	-0.370	-0.835	-1.264	-1.348
$c_{m,CFD}$	0.0001	-0.378	-0.8585	-1.1833	-1.0785

A comparison of aerodynamic coefficients for five presented angles of attack is shown in Table 3 as well as in Figures 14-16. Relatively good agreement for axial and normal coefficients has been achieved for angles of attack lower than 13º. A higher disagreement rate for the case five has been expected as flow separation was evident in this case.

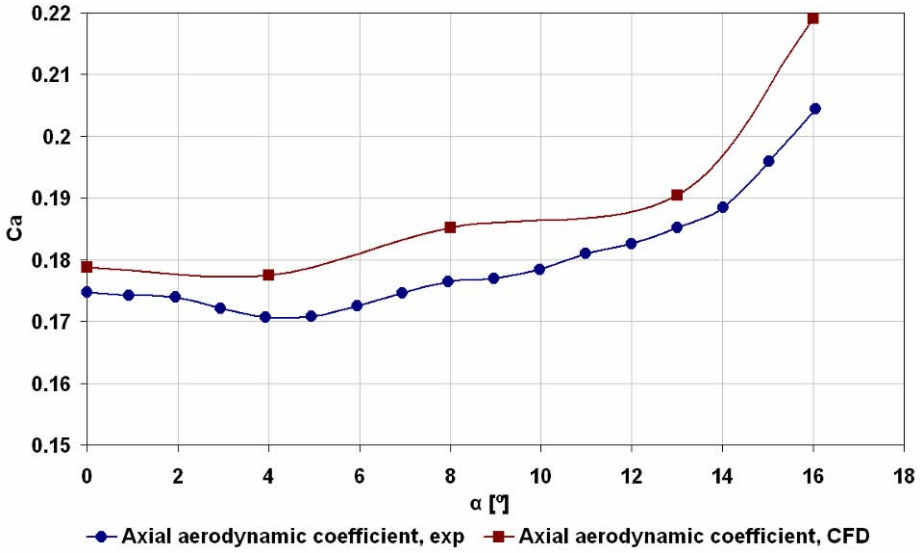

Fig. 14 Axial aerodynamic coefficient determined by experiment and CFD

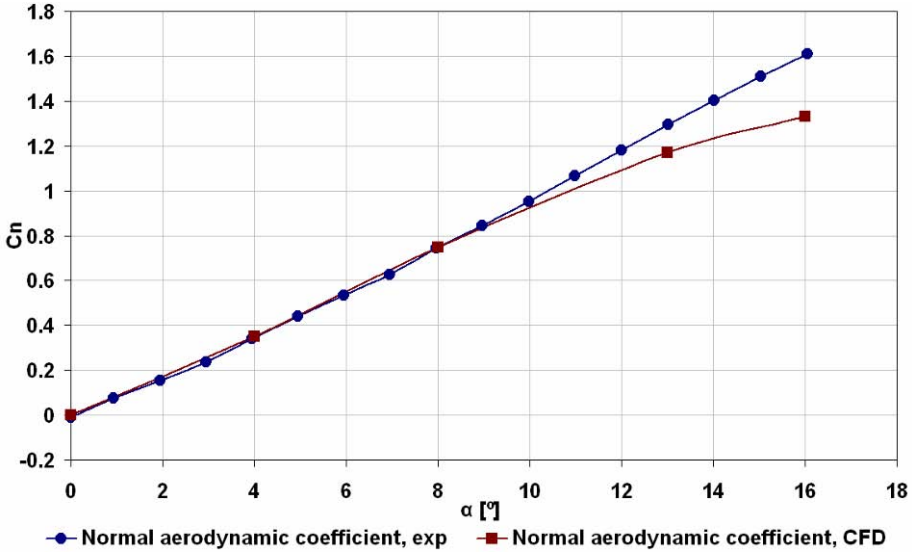

Fig. 15 Normal aerodynamic coefficient determined by experiment and CFD

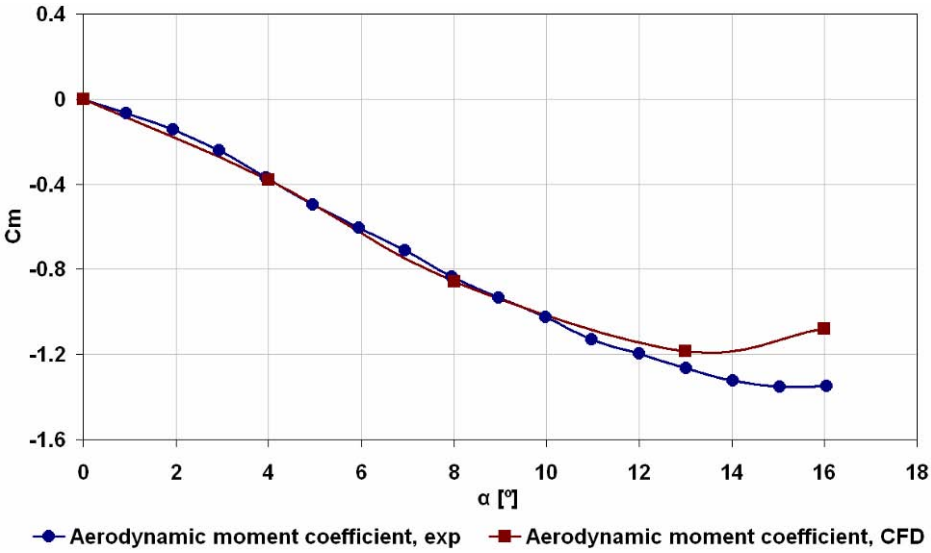

Fig. 16 Aerodynamic moment coefficient determined by experiment and CFD

9. Conclusions

Pressure distribution, base pressure and aerodynamic coefficients of a missile calibration model in a subsonic flow (M=0.6) were computationally and experimentally determined. The data for the analysis comprised of the wind tunnel tests for the range of angles of attack between 0 ° and 16° with step 1° and CFD simulation for five angles of attack: 0 °, 4°, 8°, 13°, and 16°. The results obtained by experimental means were compared to the computational data obtained with the RANS solver on an unstructured hybrid grid with a realizable k-ε turbulence model and enhanced wall treatment.

The experimental and computational pressure distribution around the model were found to be in good agreement, as well as the base pressure that was also compared, although only the area weighted average values were used in the computational approach. Computationally and experimentally determined coefficients of axial and normal forces as well as aerodynamic

moments are in good agreement for angles of attack lower than 13º. Axial aerodynamic coefficient is slightly overestimated, with the highest disagreement rate for 16 º.

In addition, the qualitative analysis of computational data of the flow behind the model base was done. The recirculation region behind the model base was captured with sufficient details required for identifying stagnation points for all investigated flow cases. The obtained computational results are found to be useful for preliminary engineering calculations, further planning of experiments which would provide an insight into the identified zones of high flow recirculation which are of special interest, as well as for the generation of appropriate, efficient computational grids for more complex numerical models capable of resolving phenomena in a base region, i.e. in the restricted domain of the present RANS simulation.

REFERENCES

[1] Moore, F.G. Wilcox, F. & Hymer T. (1994) Base Drag Prediction on Missile Configurations, Journal of Spacecraft and Rockets, Vol. 31, No.5, pp. 759-765

[2] Herrin, J.L. Dutton, J. C. (1994) Supersonic Base Flow Experiments in the Near Wake of a Cylindrical Afterbody, AIAA Journal, vol. 32, No. 1, pp. 77-83

[3] Henze, A. Glatzer, C. Meinke, M. & Schroeder W. (2011). Numerical Investigation of the Transonic Base Flow of A Generic Rocket Configuration, Modern Problems of Applied Mathematics and Mechanics: Theory, Experiment and Applications, Russia, 2011

[4] Kawai S. & Fujii K. (2007). Time-Series and Time-Averaged Characteristics of Subsonic to Supersonic Base Flows. AIAA Journal, Vol. 45, No. 1

[5] Merz R.A., Page R.H. & Przirembel N.J. (1978). Subsonic Axisymmetric Near-Wake Studies. AIAA Journal, Vol. 16, No. 7, pp. 656-662.

[6] Sahu J., DeSpirito J., Heavey K., Costello M. & Stahl J. (2009). Numerical Computations of Unsteady Aerodynamics of Maneuvering Projectiles, DoD High Performance Computing Modernization Program User Group Conference, IEEE Computer Society, pp. 88-95.

[7] Kawai S. & Fujii K. (2005) Computational study of supersonic base flow using hybrid turbulence methodology. AIAA Journal, Vol. 43, No. 6, pp. 1265-1275.

[8] Damljanović, D. Vitić, A & Vuković Đ. (2006). Testing of AGARD-B calibration model in the T-38 trisonic wind tunnel, Scientific-Technical Review, Vol. 56 No. 2, pp. 52-62

[9] Samardžić, M. Anastasijević, Z. Marinkovski, D. & Isaković (2010), J. Effects of the Sting Oscillation on the Measurements of Dynamic Stability Derivatives, Scientific Technical Review, Vol. 60, No. 2 pp. 22-26

[10] ANSYS Inc. (2009) ANSYS Fluent v12 User's Manual

[11] Shih T-H et al. (1995). A new k-ε eddy viscosity model for high Reynolds number turbulent flows, Computer Fluids Vol. 24, No. 3, pp. 227- 238.

[12] ANSYS Inc. (2009) ANSYS Fluent v12 Theory Guide

[13] Roe, P. L. (1986). Characteristic based schemes for the Euler equations. Annual Review of Fluid Mechanics, vol. 18, pp. 337-365.

[14] Akgul A., Isaković J., Mandić S., Gulay E. (2009).Determination of Base Pressure for the Agard-B Calibration Model and Comparison with an Experiment in the T-38 Wind Tunnel. Scientific Technical Review, Vol. 59, No. 2, pp.3-11

Submitted: 12.06.2012

Accepted: 15.11.2012

Slobodan Stupar
University of Belgrade,
Faculty of Mechanical Engineering,
Kraljice Marije 16,
11000 Belgrade, Serbia
Jovan Isaković
Military Technical Institute,
Ratka Resanovića 1,
11030 Belgrade, Serbia
Dragan Komarov
University of Belgrade,
Faculty of Mechanical Engineering,
Kraljice Marije 16,
11000 Belgrade, Serbia
Aleksandar Simonović
University of Belgrade,
Faculty of Mechanical Engineering,
Kraljice Marije 16,
11000 Belgrade, Serbia
Dijana Damljanović
Military Technical Institute,
Ratka Resanovića 1,
11030 Belgrade, Serbia